Combination of High-Resolution Multistage Ion Mobility and Tandem MS with High Energy of Activation to Resolve the Structure of Complex Chemoenzymatically Synthesized Glycans

David Ropartz, Mathieu Fanuel, Simon Ollivier, Adrien Lissarrague, Mounir Benkoulouche, Laurence A Mulard, Isabelle André, David Guieysse, Hélène Rogniaux

Combination of High-Resolution Multistage Ion Mobility and Tandem MS with High Energy of Activation to Resolve the Structure of Complex Chemoenzymatically Synthesized Glycans

David Ropartz, Mathieu Fanuel, Simon Ollivier, Adrien Lissarrague, Mounir Benkoulouche, Laurence A. Mulard, Isabelle André, David Guieysse, and Hélène Rogniaux*

ABSTRACT: Carbohydrates, in particular microbial glycans, are highly structurally diverse biomolecules, the recognition of which governs numerous biological processes. Of special interest, glycans of known monosaccharide composition feature multiple possible isomers, differentiated by the anomerism and position of their glycosidic linkages. Robust analytical tools able to circumvent this extreme structural complexity are increasing in demand to ensure not only the correct determination of naturally occurring glycans but also to support the rapid development of enzymatic and chemoenzymatic glycan synthesis. In support to the later, we report the use of complementary strategies based on mass spectrometry (MS) to evaluate the ability of 14 engineered mutants of sucrose-utilizing α-transglucosylases to produce type/group-specific *Shigella flexneri* pentasaccharide bricks from a single lightly protected non-natural tetrasaccharide acceptor substrate. A first analysis of the reaction media by UHPLC coupled to high-accuracy MS led to detect six reaction products of enzymatic glucosylation out of the eight possible ones. A seventh structure was evidenced by an additional step of ion mobility at a resolving power (R_p) of approximately 100. Finally, a R_p of about 250 in ion mobility made it possible to detect the eighth and last of the expected structures. Complementary to these measurements, tandem MS with high activation energy charge transfer dissociation (CTD) allowed us to unambiguously characterize seven regioisomers out of the eight possible products of enzymatic glucosylation. This work illustrates the potential of the recently described powerful IMS and CTD−MS methods for the precise structural characterization of complex glycans.

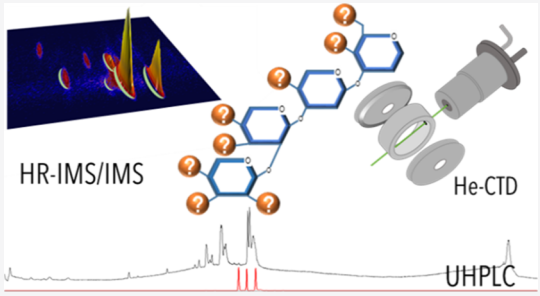

INTRODUCTION

The composition and structure of carbohydrates offer a tremendous diversity. This diversity arises from the variety of monosaccharides, D- and L-oses, the open and cyclic forms (tautomerism, i.e., furanose or pyranose forms), the α/β anomerism of the glycosidic bond, and the number and position of modifications. As shown by Laine,[1] the number of possible isomers calculated for reducing hexasaccharides composed only of D-hexoses, including linear and branched forms, is above 10^{12}. The identification of precise glycosylation patterns creates a highly specific language, known as the glycocode.[2] In the living cell, the glycome (composed by cell surface glycans and secreted glycans) is the less conserved biomolecule of evolution. However, while featuring the largest informational diversity, it remains very far behind the genome, the transcriptome, the proteome, the metabolome, and the lipidome in terms of knowledge base.[3]

The extreme structural variability allows glycans and glycoconjugates to modulate or mediate a wide variety of functions in physiological and pathophysiological states.[4] Indeed, slight changes in glycosylation strongly impact many biological processes in health and disease. Immune receptors from the host recognize glycans present on the surface of pathogens including bacteria or viruses.[4] Conversely, the glycans of a pathogen can mediate adhesion to host cells and subsequent invasion by means of highly specific interactions.[5] In addition, glycans can act as a mechanical barrier against infection.[6] Otherwise, glycan-dependent epitopes is a well-established concept. These unique properties have generated strong interest in the search for glycan-based therapeutics.[7] In particular, outstanding developments include vaccines against bacterial infections.[8] Over the past decades, the strategy was investigated in the context of shigellosis.[9] Interestingly, going beyond the use of polysaccharide antigens purified from bacterial cell cultures, the development of synthetic glycan-based vaccines is actively explored in the field of cancer and

infectious diseases,[10] including that of shigellosis.[11,12] Up front, the main challenge is to define the structure of the relevant biologically active glycoforms. Subsequently, another hurdle consists in ensuring the correct chemical and/or enzymatic synthesis of specific analogues so as to develop unique glycan-based therapeutics. This requires the development of robust, sensitive, fast, and efficient analytical approaches tolerant to crude mixtures such as biological samples.

Compared to those available for other classes of biomolecules, robust easy-to-implement analytical methods to assess the glycan structures are still lacking. Nuclear magnetic resonance (NMR), which is very informative, often requires time-consuming and complex purification steps to obtain significant quantities of high-purity material. Contrariwise, mass spectrometry (MS) requires low amounts of material and can decipher complex samples when coupled with appropriate separation techniques. The fields of proteomics, metabolomics, and lipidomics have greatly benefited from the contribution of the developments in MS combined with ultrahigh-performance liquid chromatography (UHPLC). Unfortunately, important limitations prevent an optimal use of MS in glycosciences as detailed hereafter.

Upstream of MS, many techniques were developed for the separation of glycans. A recent review[13] highlights that the use of a single separation method is inappropriate due to the complex nature of carbohydrates. Among the many approaches that were discussed, capillary electrophoresis and nano-/microfluidics still lack the ability to separate complex mixtures of carbohydrate isomers. The authors conclude that liquid chromatography offers better capacities to that aim. Among the suitable stationary phases, porous graphitized carbon (PGC) at high temperature provides the most comprehensive results albeit requiring a derivatization strategy. Ion mobility spectrometry (IMS) was also discussed as an alternative or a complement to conventional approaches. This method allows us to separate ions according to their conformations in the gas phase. The major limitation for discriminating carbohydrate isomers was linked to the low resolving power reachable until recently on commercial instruments. Reyes et al.[13] point out two recent and major advances in the field of IMS based on traveling wave IMS (TWIMS)[14] which can overcome this limitation. The first, named structure for lossless ion manipulation (SLIM), was introduced by the group of R.D. Smith in 2014.[15] More recently, the same group introduced the SLIM SUPER IM−MS technology, a printed circuit board with a total ion trajectory close to 13 m that allows us to obtain a resolving power (R_p) of ∼400−600.[16] The potential of the system was demonstrated with the correct determination of isomer mixtures from monosaccharides to pentasaccharides in a rapid timescale (<1 s).[17,18] The second disruptive technology, initially called cyclic IM device, was launched by Waters Corp. (Wilmslow, UK) also in 2014.[19] The instrument, which uses a cyclic TWIMS cell placed orthogonally to the trajectory of the ions,[20] was commercialized as "SELECT SERIES Cyclic IMS" by Waters. It primarily allows ions to go through multiple passes in the ion mobility cell in order to increase the separation path and thereby, the resolving power ($R_p \approx 100.\sqrt{n}$ with n, the number of passes).

The SELECT SERIES Cyclic IMS is a very attractive platform for structural studies of molecules with an isomeric barrier as it allows multistage experiments, named IMS^n, as well as pre- and post-IMS fragmentation (for a review of tandem IMS history, see[21]). Ujma et al.[22] demonstrated the capacity of the instrument to separate three isomers of pentasaccharides and for each of them to separate between their α and β anomers and the open-ring conformation of the reducing end. In this work, the anomeric information was retained by the Y-type fragments after an IMS/IMS step. In a further study, our group showed that the instrument allowed us to unveil the fine structure of complex sulfated glycans in a crude enzymatic digestion medium of the cell wall of a red algae.[23] In this study, resolving power of up to 920 was achieved, and a multistage strategy was used to confirm certain sulfated isoforms. Recently, we further demonstrated the significant potential of this technology for glycosciences. We proved that IMS^n allows us to characterize the anomerism of the glycosidic bond, allowing the de novo characterization of the anomerism of unknown oligosaccharides.[24] We also introduced a new concept for the organization of data in glycomics based on molecular networks built from the high-resolution IMS/IMS information.[25] This concept allows us to classify families of glycan structures depending on all their isomeric specificities—the anomerism, the epimerism, and the branching pattern. Cyclic IMS was also recently used successfully to characterize the *O*-glycosylation of a transmembrane SARS-CoV-2 glycoprotein.[26] This approach was also recently demonstrated using the SLIM technology combined with cryogenic vibrational spectroscopy to discriminate a mixture of two positional isomers of fucose.[27]

However, even at high resolution, IMS alone can only determine structures if the appropriate standards are available. To explore the structure of unknown products and go beyond the limits of standard synthesis, tandem MS was and remains a method of choice. However, the most popular approach in tandem MS—low-energy collision-induced dissociation (LE-CID)—produces mainly fragments issued from the cleavage of glycosidic linkage and, in contrast, few cross-ring. For many structural isomers (e.g., structures with a strong symmetry of the reducing and nonreducing ends, or positional isomers), the m/z information of these fragments alone is not sufficient to assign unambiguously the complete structure of glycan isomers. Nonetheless, the production of cross-ring fragments, which generally bear less ambiguous information, can be improved using radical driven fragmentation involving ion−electron interactions,[28] ion−photon interactions (VUVPD, XUVPD),[29] or ion−ion interactions. Among the ion−ion interaction approaches, charge transfer dissociation (CTD) shows a great efficiency for the structural characterization of diverse carbohydrates in a time scale compatible with UHPLC.[30−33] As demonstrated in these studies, CTD produces rich patterns of fragments with many intracyclic fragments, which allow the determination of the branching pattern and the localization of modifications, including labile ones such as sulfate- or methyl-esters by maintaining these modifications on many fragments.[30,31,33]

In the present work, complex pentasaccharides obtained from the enzymatic α-D-glucosylation of a non-natural lightly protected tetrasaccharide acceptor were structurally characterized. A collection of 14 computer-aided engineered mutants of branching sucrases from the glycoside hydrolase family 70 (GH70) were selected for their ability to produce specific building blocks involved in the synthesis of haptens representative of the O-antigen of prevalent serotypes of *Shigella flexneri* (SF).[34,35] This family of bacteria is responsible for shigellosis, one of the most critical enteric diseases in children under five in low and middle income countries, and

one for which there is no licensed vaccine.[36,37] Reaction media were studied using a unique multipass high-resolution IMS setup and CTD activation, both combined with a PGC–UHPLC strategy. Our results show that the emergent methods proposed in this workflow are powerful technologies that can be used to screen complex mixtures and to identify the fine structure of specific glycans with a very high level of certainty, as required in biopharma. They pave the way forward to novel appropriate tools to circumvent existing analytical limitations in glycosciences.

EXPERIMENTAL SECTION

Samples. Crude reaction mixtures of pentasaccharides were obtained from the glucansucrase mutant-mediated α-D-glucosylation of the chemically synthetized tetrasaccharide ABC′D′ (Figure 1) as described previously.[38] Biocatalysts used for generating the samples studied in this work were described previously.[34,35]

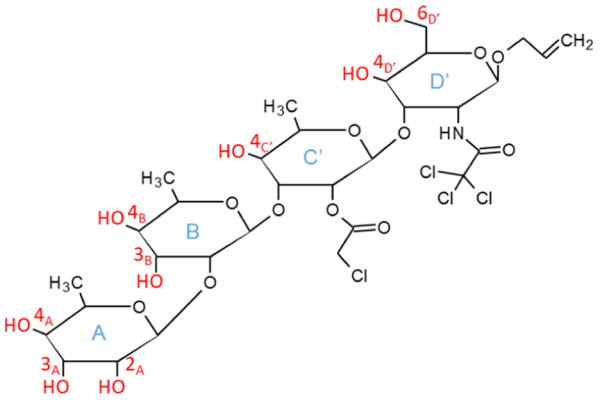

Figure 1. Selected ABC′D′ tetrasaccharide acceptor substrate, showing the eight potential sites of enzymatic transglucosylation (in red).

Chemicals. HPLC grade acetonitrile (ACN) was purchased from Carlo-Erba. Ultrapure Water was obtained from a Milli-Q apparatus (Millipore).

MS and Ion Mobility MS (IMS). Acquisitions were performed on a Select Series Cyclic IMS (Waters, Wilmslow, UK). Briefly, this instrument can be described as a Q-TOF mass spectrometer in which a cyclic traveling wave ion mobility (TWIM) cell is mounted between the quadrupole and the TOF analyzer and in-between two collision cells (called "trap" and "transfer" cells). Instrument design and operations were described by Giles et al.[20] Spectra were recorded in the positive electrospray ionization (ESI) ionization mode in the m/z range 150–1200, with the TOF operating in the V-mode. The source parameters were the following: capillary voltage 2.8 kV; cone voltage 150 V; source temperature 100 °C; desolvation temperature 280 °C; desolvation gas 600 L/h; and nebulization gas 6 bar. Cyclic TWIM was performed with a wave height of 22 V and a wave velocity of 375 m/s. Transfer parameters were the following: pretransfer guide gradient 7.0 V; pretrans bias 0.0 V; transfer entrance 2.0 V, transfer gradient 4.0 V, and transfer exit 15 V. The cyclic TWIM allows us to perform several passes. For IMS measurements, the data acquisition sequence is designed by selecting specific functions at a chosen time point.[20] For the data acquired in IMS with one pass, the sequence was the following: inject 10 ms; separate 17 ms; eject; and acquire 13.20 ms. The instrument also allows us to perform experiments in which ions are selected in a defined IMS arrival time (AT) window, while ions lying outside the window are selectively ejected from the TWIM cell—called IMS/IMS experiments or "head and tail" experiments. For IMS/IMS, molecules were separated first with a one-pass sequence (similar as above) and then selected according to their mobility and allowed to go for another four-pass separation in the TWIM cell. The sequence is illustrated and detailed in Figure S1. The quadrupole was used as a filter to select the m/z of the ion of interest, with a window width of 4 Da so as to keep the isotopes of the molecule. The mobility spectra were recorded with the Quartz software (Waters embedded analyzer, release 5). Data were processed using MassLynx 4.2, UNIFI 1.9, and Driftscope 2.9 (all from Waters, Wilmslow, UK). For the measurements of the AT distributions and the integration of the mobility peaks, the extracted ion mobility spectra were smoothed [window size (scan) ±1, number of smooths: 3, and method: mean].

Tandem MS by Helium-CTD (He-CTD-MS/MS). Acquisitions were performed on an amaZon SL 3D ion trap mass spectrometer (Bruker Daltonics, Bremen, Germany) modified for CTD experiments.[39] Briefly, the ion trap was interfaced with a saddle field fast ion source (VSW/Atomtech, Macclesfield, UK) with helium as the CTD reagent gas. High voltage was applied using a high voltage generator (ION tech Ltd, Oldbury, UK). In order to synchronize the ion trapping for MS/MS with the introduction of the helium plasma into the ion trap, the trapping event was used to trigger a waveform generator (series Keysight 33600A, irradiation time set to 200 ms) and a modified high voltage switch (HTS 151-03-GSM, BEHLKE). The helium flow from the ion gun was adjusted to get a vacuum of ~1.2×10^{-5} mbar in the trap chamber. The helium plasma was continuously verified by measuring the induced current in the ion gun. Compared to the setup described by Hoffmann and Jackson,[39] the hole in the ring electrode was increased to 4 mm in diameter in order to achieve higher fragmentation efficiency. The electrospray source parameters were the following: capillary voltage: 4.5 kV; nebulizer gas: 7.3 psi; and dry gas: 4 L/min (80 °C). Mass spectra were recorded in the positive ionization mode in the m/z range 250–1200. Precursor ions were isolated with a window width of 4 Da. The activation time was 200 ms. Data were processed using Data Analysis 4.4 (Bruker Daltonics, Bremen, Germany), MSConvert 3.0.18261,[40] and mMass 5.5.0.[41] Acquisition blanks were performed by recording spectra with a capillary voltage set at 500 V (i.e., too low voltage to ionize).

Ultrahigh-Performance Liquid Chromatography. The two mass spectrometers used in this work were coupled with the UHPLC system (Acquity H-Class Plus or Acquity H-Class, both from Waters, Manchester, UK). The chromatographic separations were performed on a Hypercarb column (100 × 1 mm, particle size 3 μm, Thermo-Fisher Scientific, Courtaboeuf, France) heated at 80 °C. The flow rate was 0.165 mL min^{-1}. A binary gradient was performed during 47 min (A: H_2O, B: ACN). The gradient started with 8 min at 95.5% of A and then ramped linearly to 80% of B in 22 min and stayed at 80% of B during 12 min; initial conditions were restored during the last 5 min. Samples were diluted in 95.5% A, with a factor of 200 for LC–IMS experiments and a factor of 10 for LC-He-CTD–MS/MS experiments. Five microliters were injected in both cases.

RESULTS AND DISCUSSION

Despite major improvements over the years, the chemical synthesis of oligosaccharides remains challenging. Conventional strategies often involve fine-tuned orthogonally protected building blocks so as to differentiate between multiple reactive hydroxyl groups and achieve the required regioselectivity upon glycosylation. Otherwise, controlling stereoselectivity might be an issue especially in the case of 1,2-*cis*-glycosylation as required in the synthesis of SF oligosaccharides. Indeed, most SF O-antigens share the same backbone, defined by a unique α-L-rhamnopyranosyl-(1 → 2)-α-L-rhamnopyranosyl-(1 → 3)-α-L-rhamnopyranosyl-(1 → 3)-2-*N*-acetyl-2-deoxy-β-D-glucopyranosyl tetrasaccharide core (ABCD). Type/group specificity resides in part in the location of an α-D-glucosyl residue (E) on the ABCD core.[42] To overcome limitations related to chemical 1,2-*cis*-glucosylation while aiming at a panel of synthetic type-specific SF oligosaccharides, Hu and co-workers[38] proposed a chemoenzymatic strategy involving an enzymatic α-D-glucosylation step. The implemented strategy relied on the design and synthesis of a single lightly protected tetrasaccharide analogue of the O-antigen backbone repeating unit (ABC′D′), namely, allyl α-L-rhamnopyranosyl-(1 → 2)-α-L-rhamnopyranosyl-(1 → 3)-2-*O*-chloroacetyl-α-L-rhamnopyranosyl-(1 → 3)-2-deoxy-2-trichloroacetamido-β-D-glucopyranoside (Figure 1), which was used as the common acceptor precursor to all required glucosylation patterns.[38] As shown, the acceptor substrate for the α-D-glucosylation reaction—ABC′D′—displays eight sites that can potentially be modified. Having achieved the selective enzymatic α-D-glucosylation at OH-3_A of ABC′D′ by means of six wild-type branching sucrases, we then reported the computer-aided engineering of BRS-B, a GH70 branching sucrase. Using an enzyme design protocol based on the sampling of mutations on 27 positions and a Rosetta design-based approach, 12 sequences were selected depending on the SF serotype-specific pentasaccharide products: M6 and M14 (SF type I); M18, M21, M23, M28, M30, M31, and M34 (SF2a serotype); M35, M40, and M41 (SF3a serotype).[34] To characterize the exact activity of these enzymes, a combination of RP−HPLC−UV, RP−HPLC−high-resolution mass spectrometry and NMR was used. This complex approach led to the identification of multiple glucosylation products per enzymes. Analysis revealed glucosylation of ABC′D′ at OH-$6_{D'}$, which corresponds to the glucosylation pattern characteristic of SF-type factor IV. Pentasaccharide ABC′(E1 → 6)D′ was the main product of a native GH70 branching sucrase BRS-B Δ1.[38] Two additional compounds, (E1 → 4)ABC′D′ and (E1 → 3)ABC′D′, the latter representing SF group factor O7,8, as present in the SF3a O-antigen were identified. As an attempt to characterize the formed products further, we studied mutants M35 and M40 by PGC−HPLC−MS/MS (classical approach using LE-CID). In addition to confirming the previous structures, we hypothesized glucosylation at OH-2_A ((E1 → 2)ABC′D′) by M35 and at OH−3_B [A(E1 → 3)BC′D′] by M40. Interestingly, the later pattern defines SF-type factor V. Unfortunately discriminating between these two isomers was impossible due to the lack of informative fragments.[34]

In order to refine our understanding of the products of ABC′D′ enzymatic α-D-glucosylation, the 14 reaction media issued from the independent reaction of ABC′D′ with the 12 mutants designed from the GH70 branching sucrase BRS-B[34] and 2 mutants from the GH70 branching sucrase ΔN_{123}-GBD-CD2, F2163G named G and W2315S-F2136L named SL,[35] were studied using advanced MS-based approaches.

UHPLC−MS Analysis of the Enzymatic Reaction Media. The expected product of ABC′D′ enzymatic α-D-glucosylation is a pentasaccharide corresponding to one glucosyl residue transferred on either one of the eight ABC′D′ hydroxyl groups. The expected neutral mass is of 1039.20 Da, from which the $[M + Na]^+$ and $[M + K]^+$ species (i.e., the two main alkali ionic species expected in ESI MS) have *m/z* of 1062.19 and 1078.20, respectively. Extracting the ion chromatogram for both ions revealed six retention times (RTs) along the chromatographic gradient for which unambiguous signature of both *m/z* were detected, as exemplified for sample M30 (Figure S2). However, looking carefully at the data, other features with *m/z* overlapping with the targeted ones are detected along the gradient, albeit with lower intensities (exemplified in Figure S2 by the three spectra at the bottom right). None of these features has the characteristics (ions relative abundances and/or isotope profiles) expected for the reaction product (i.e., the concomitant presence of 1062.19 and 1078.20 *m/z*). We thus considered they were impurities of the reaction medium. One of the spectra has yet a clear ionic pattern (RT 25.4 min, Figure S2), suggesting a contaminating product with a mass of 16 Da less than that of the target product (neutral mass of 1023.20 Da, herein detected as $[M + Na]^+$ and $[M + K]^+$ species at *m/z* 1046.20 and 1062.17, respectively). For that reason in order to focus on the ions corresponding to the expected monoglucosylated ABC′D′ pentasaccharides, the chromatographic peaks to be analyzed in detail in the following were those for which the two theoretical cationic forms (*m/z* 1062.20 and 1078.20) specific to the intended product were clearly present. In the ion chromatogram recorded for sample M30 (Figure S2), the six eluting compounds with RTs of 21.5, 22.2, 22.5, 23.0, 23.4, and 24.6 min fulfilled the criteria. The results obtained for the 14 reaction media are summarized in Table 1.

Among the eight theoretical monoglucosylated products, six possible isoforms were detected eluting at six different RTs (labeled ① to ⑥). From this analysis, one can see that each reaction medium contains at least one of these isoforms. Structures ①, ②, ④, and ⑥ had higher intensities than structures ③ and ⑤. Possible additional isoforms were evidenced by shoulders in the ion chromatogram, for example, after peak ④ in samples M40 and G (data not shown).

Refined Separation and Quantification of the Isoforms Detected for the Pentasaccharide by High-Resolution Ion Mobility. The shape of some peaks in the previous UHPLC−MS profiles suggested that additional pentasaccharide isoforms of the pentasaccharides may be present in the reaction mixture but that they were not separated or not detectable at this point. To circumvent this limitation, an additional dimension of analysis—high-resolution IMS—has been used in conjunction with UHPLC and MS.

The SELECT SERIES Cyclic IMS was used in the first place with a single pass in the ion mobility cell (estimated $R_p \approx 100$) to analyze each sample. As exemplified for M35 (Figure 2), in addition to the three conformations found by use of UHPLC−MS (Table 1), a fourth conformation was detected, which coeluted with species ② (RT 22.2 min) in the UHPLC chromatogram. Indeed, two isoforms were detected in the

Table 1. Isomers of Monoglucosylated ABC′D′ Detected by UHPLC−MS Analysis in the 14 Reaction Media[a]

Reaction media	Species ID	①	②	③	④	⑤	⑥
	RT	21.5	22.2	22.5	23.0	23.5	24.6
M6			X		X	x	X
M14							X
M18							X
M21		X	X	x	X		X
M23		X	X		X		X
M28			X				X
M30		X	X	x	X	x	X
M31					X		X
M34		x	X		X		X
M35		X	X		X		
M40		X	X		X*		x
M41		X	X		X	X	X
SL		X	X		X	x	X
G		X	X	x	X*		X

[a]X: major compound—X: minor compound—x: traces—*: shoulder observed on the chromatographic peak; RT: retention time (min). M6-M41 are mutants of BRS-B,[33] while SL and G are mutants of GBD-CD2.[34]

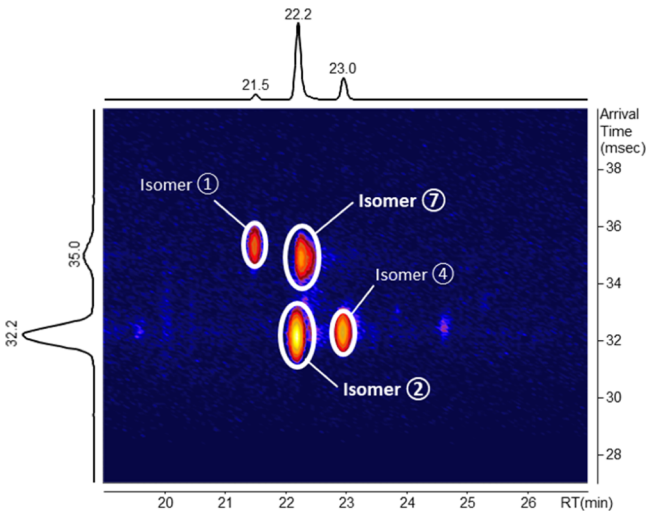

Figure 2. 2D map (RT vs AT in ion mobility) of the extracted ion chromatogram at m/z 1062.2 ± 0.1 from sample M35. The two isomers coeluting in UHPLC (② and ⑦) are indicated in bold.

chromatographic peak eluting at 22.2 min, with ATs in ion mobility of 32.21 and 35.04 ms, respectively. The additional species was named ⑦. Overall, the IMS chromatograms of the 14 samples followed the same trend. Independently of the RT in UHPLC, two groups of isoforms with different ion mobilities could be emphasized, with ATs of 32.1 and 35.2 ms, respectively (Figure S3). In order to improve the ion mobility separation and achieve higher R_p, the groups were separated based on their ion mobility and individually subjected to an additional IMS. This so-called IMS/IMS strategy (Figure S1) was performed in combination with UHPLC. The fastest group (arriving at 32.1−32.6 ms after one pass in ion mobility) was subjected to an additional separation over 72 ms, while the slowest group (arriving at 35.0−35.3 ms after one pass) was subjected to a separation over 82 ms. A theoretical IMS resolving power of $R_p \sim 250$ was achieved. Integrating the RT and ion mobility data of the two-dimensional (2D) plots for all samples led to define eight different species (named ① to ⑧) by their RT and AT in ion mobility (Table 2). This means that, thanks to the longer path of separation in the IMS/IMS experiments (six passes through the cyclic IM cell), not just one—as originally hypothesized—but two additional species (species ⑦ and ⑧) were detected when compared to UHPLC−MS detection (Table 1). Importantly, because the separation among the glucosylated species was improved, as exemplified for M41 (Figure S4), a more accurate quantification of the relative amount of each species in the different samples could be derived (Table 2).

The UHPLC−IMS/IMS analysis also confirmed the presence of contaminating species in the samples (Figures S5 and S6, spots annotated with Greek letters). These contaminants had ions within the selection window of the quadrupole (m/z 1062.2 ± 0.1) and yielded several signals in the 2D plots, as exemplified for sample M18 (Figure S6), However, none of them displayed the characteristic signature of the targeted product (i.e., two ions at 1062.2 and 1078.2 m/z); of note, some of those (α, δ, γ, and ζ) displayed a doublet at m/z 1046.19 and m/z 1062.19 and may be related to the aforementioned contaminating product whose mass is 16 Da lower than that of the intended ABC′D′E product. The other ones (β, ε, and η) are present as traces and their patterns are difficult to interpret, but clearly, they do not seem to match with the isotopic pattern expected for the monoglucosylated ABC′D′. As shown in the different 2D plots recorded for the 14 analyzed samples, all eight possible isoforms corresponding to the different pentasaccharides obtained by enzymatic glucosylation of the ABC′D′ acceptor substrate were unequivocally detected and separated from other species with the higher resolution in ion mobility achieved in these IMS/IMS experiments.

Structural Determination of the Pentasaccharide Isomers by UHPLC-He-CTD-MS. The UHPLC−CID MS/MS experiment was conducted in order to assign the structure of each isomer. For each product, the tandem MS spectra showed predominant losses on the reducing end. A few inter-osidic cleavages including consecutive fragmentation were also observed. This is illustrated for three structures (①, ②, and ④) in Figure S7, with the loss of the chloroacetyl group at OH−$2_{C'}$ and of the trichloroacetyl group at OH-$2_{D'}$ colored in green and in red, respectively. These data could not be used to distinguish between isomers and assess their respective structure. Especially, they did not allow us to draw information on the regioselectivity of the branching. Instead, a strategy based on UHPLC-He-CTD-MS was implemented to characterize the exact structure of each compound. Ion mobility was not accessible on the setup. However, based on the data extracted from the UHPLC−IMS/IMS−MS chromatograms, specific samples were selected for further analysis. Each species was characterized in a reaction medium where its quantification is the most significant, taking into account the possible presence of co-eluted species.

The structures of the major species were determined using the sample in which they were most intense in the absence of any coeluting species, and subsequently confirmed by analysis of the same product formed in a second sample. The structures of the most intense isomers ①, ②, and ④ were defined in samples M21, M30, and M6, respectively (UHPLC-He-CTD spectra and annotated structures are shown in Figures S8−S10, and subsequently confirmed in samples M40, M21, and M30,

Table 2. Isomers and Relative Quantification Highlighted by UHPLC−IMS/IMS−MS Analysis with Detailed AT for Each Isoform (in msec)[a]

Reaction media	①	②	⑦	③	④	⑧	⑤	⑥
RT	21.5	22.2	22.2	22.5	23.0	23.2	23.5	24.6
AT	127.1	112.0	125.4	112.2	112.6	114.8	112.7	113.7
std dev	0.098	0.089	0.042	0.035	0.12	0.075	0.075	0.061
M6		3.2E+04			**6.9E+05**	4.2E+03	1.1E+04	1.8E+04
M14								1.6E+04
M18								2.8E+04
M21	**2.7E+05**	**2.5E+05**		5.2E+03	**2.0E+05**	8.7E+03		1.4E+04
M23	1.4E+04	**1.2E+05**			**2.7E+05**			9.7E+03
M28		6.0E+03			5.3E+03			2.6E+04
M30	4.1E+04	**3.5E+05**		1.1E+04	**7.0E+05**	1.2E+04	8.8E+03	2.4E+04
M31					1.9E+04			3.8E+04
M34	3.7E+03	8.9E+04			**1.9E+05**	3.1E+03		2.6E+04
M35	1.2E+04	**1.2E+05**	7.6E+03		5.9E+04			1.5E+03
M40	**2.3E+05**	**1.6E+05**			**5.1E+05**	5.1E+04		8.9E+03
M41	**1.5E+05**	7.6E+04			**7.3E+05**	1.2E+04	8.9E+03	2.8E+04
SL	7.2E+04	**1.1E+05**			**7.7E+05**		8.3E+03	1.8E+04
G	1.7E+04	**3.6E+05**	7.0E+02	1.1E+04	1.7E+05	1.4E+04		2.0E+04

[a]RT = retention time; AT = arrival time; std dev = standard deviation calculated for the AT of a given species. M6-M41 are mutants of BRS-B,[33] while SL and G are mutants of GBD-CD2.[34] In red: major species in the sample. In bold: species with an area greater than 1.0×10^5.

respectively. In the species ①, ②, and ④, the ABC′D′ backbone was α-D-glucosylated on OH−4_B, OH-4_A, and OH-$6_{D'}$, respectively. Whereas the A(E1 → 4)BCD ① and (E1 → 4)ABCD ② motifs are yet unreported, the (E1 → 6)D branching pattern as seen in ABC(E1 → 6)D ④ is characteristic of the type factor IV in the SF classification.[42] For isomer ⑦, due to the coelution with isomer ② in UHPLC, we integrated the time area estimated from the IMS/IMS data in sample M35. After a baseline subtraction, the signal was normalized according to the intensity of the precursor ion at *m/z* 1062.2 obtained for isomer ② in sample M30 in He-CTD. Most of the observed fragments are shared between the two isomers, indicating that glucosylation must have occurred, as for isomer ②, on a nonreducing end residue. However, specific peaks were found in the area *m/z* 780−1050 (Figure S11). The obtained pattern allowed us to conclude that isomer ⑦ was the (E1 → 2)ABC′D′ pentasaccharide issued from the transglucosylation of ABC′D′ at OH-2_A (Figure 3). Identifying isomers ⑥, ③, and ⑤ was more challenging due to the low intensity of the fragments. Merging the data acquired from three different samples (each after a blank subtraction) circumvented the issue. The spectrum for isomer ⑥ (Figure S12) was obtained by merging data collected for samples M18, M28, and M31. The analysis shows that the glucosylation occurs on the D′ subunit (fragments $^{0,2}X_1$, $^{1,5}X_1$, Y_1, Y_1'', and Z_1, respectively at *m/z* 666.2, 576.1, 548.1, 546.1, and 530.1). However, no intracyclic fragment unambiguously validates the precise localization of glucosylation. However, as the position (E1 → 6)D′ has been validated for isomer ④ (Figure S10) and considering that the enzyme, a glucansucrase that acts along a mechanism of retention of configuration, is specific for an α-D-glucosylation, we concluded that this isomer (⑥) features the (E1 → 4)D′ branching characteristic of SF-type factor I as present in the O-antigens of SF serotypes 1a, 1b, 1d, 7a, and 7b, respectively.[42,43] The spectra of isomers ③ and ⑤ were

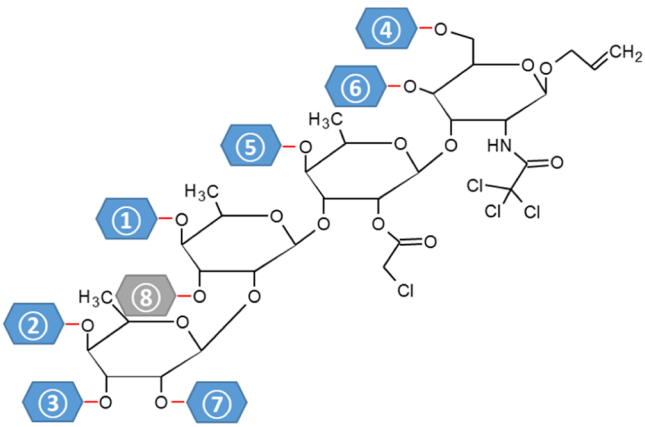

Figure 3. Summary of the structures of the pentasaccharide isomers deciphered in all samples. In blue, the structures validated by UHPLC−CTD−MS. In gray, the last structure, deduced from the others.

obtained by merging data collected for samples M21, M30, and G and from samples M6, M41, and SL, respectively (Figure S13). The spectrum for isomer ③ mainly contained the major fragments Y_n and $^{1,5}X_n$, which restricted the extractable information. Nevertheless, these fragments indicate that glucosylation occurred on the A subunit (fragments $^{1,5}X_3$, Y_3, Z_3, and B_1 at *m/z* 782.4, 754.1, 735.9, and 331.1, respectively). Again, no intracyclic fragment validates the exact localization of the glucosylation. The positions OH-2_A and OH-4_A being already assigned to, respectively, isomer ② (Figure S9) and isomer ⑦ (Figure S11) and assuming again that the enzyme is specific for an α-glucosylation, isomer ③ was deduced to be glucosylated at OH-3_A of tetrasaccharide ABC′D′ to give the group factor 6,7 as found in the O-antigens of SF3a [(E1 → 3)AB_{Ac}CD] and SFX [(E1 → 3)ABCD] as well as in those of SF2b [(E1 → 3)AB(E1 → 4)CD] and SF5b [(E1 → 3)A(E1

→ 3)BCD], which feature a di-*O*-glucosylated ABCD hexasaccharide repeating unit.[42,43] In contrast, isomer ⑤ was unambiguously characterized by UHPLC CTD analysis. The observation of fragments 1,5X2, Y2, 2,4X1, 1,5X1, and Y1 (respectively at *m/z* 798.0, 770.1, 548.1, 414.0, and 386.1) defined this product of ABC′D′ enzymatic *α*-*d*-glucosylation at $OH-4_{C'}$, providing the type factor II pattern (E1 → 4)C, as found in the O-antigens of SF2a [AB(E1 → 4)CD] and SF2b, which also has a di-*O*-glucosylated repeating unit [(E1 → 3)AB(E1 → 3)CD].[42,43]

The last regioisomer, structure ⑧, was present in only minute amounts in the different samples. Moreover, the low intensity of the signals was conjugated with the presence of a major coeluted species (isomer ④), which prevented any direct assignment from the UHPLC CTD data. However, because seven out of the eight possible regioisomers were precisely identified from experimental data, we postulate that this compound ⑧ results from the transglucosylation of ABC′D′ at $OH-3_B$. The (E1 → 3)B branching pattern is associated to the type factor V in the SF classification. It is found in the O-antigens of SF5a and SF5b, which encompasses the A(E1 → 3)BCD pentasaccharide and (E1 → 3)A(E1 → 4)BCD hexasaccharide repeating units, respectively.[42] The structures of the eight possible regioisomers resulting from the glucansucrase-mediated glucosylation of ABC′D′ are compiled in Figure 3. All these pentasaccharides were identified in the frame of this work.

CONCLUSIONS

In order to understand the biological functions of oligosaccharides and to ensure the full exploitation of their functional properties, in particular in Health science, their complete structural characterization is essential. It is both important to identify compounds of interest but also to demonstrate our ability to produce them in a controlled and batch to batch repeatable manner.

In the present study, 14 enzymatic reaction mixtures were studied for their ability to contain lightly protected pentasaccharides comprising the *α*-D-glucosylation patterns found in the repeating units of a diversity of SF O-antigens. The targeted pentasaccharides were the products of glucansucrase-mediated transglucosylation of a non-natural chemically synthetized ABC′D′ tetrasaccharide acceptor designed to maximize the number of possible monoglucosylation patterns, in fact up to eight. The transglucosylation products were discriminated and quantified in all 14 reaction samples using UHPLC−IMS*n*−MS. After one pass (R_p ∼ 100), we detected one additional feature when comparing to UHPLC−MS data (species ⑦). By increasing the resolving power to about 250 (six passes, with a slicing experiment), an eighth structure could be evidenced (species ⑧). In fact, the higher separation path and resolving power achieved an efficient definition of the three species ④, ⑤, and ⑧ which partially overlapped after one pass. In addition to allowing the detection of additional features, the higher IM resolving power also improved the accuracy of the quantification of each feature relative to the others. Seven out of the eight expected pentasaccharides were precisely characterized by CTD−MS, whereas the structure of the last isomer was deduced from the whole set of available data. This experimental design allowed us to directly characterize the enzymatic production of all five glucosylation patterns characteristic of SF type and group factors, leading to pentasaccharide building blocks that could be used in the synthesis of oligosaccharides representative to at least 13 different SF serotypes, identified on the basis of a monoglucosylated ABCD pentasaccharide repeat (types 1a, 1b, 2a, 3a, 4a, 4b, 5a, and X) or a diglucosylated ABCD hexasaccharide repeat (types 1d, 2b, 5b, 7a, and 7b).

These results, which have been achieved through the combined use of the latest high-resolution IMS and CTD MS/MS technologies and could not have been achieved otherwise, pave the way for future developments in the field of *Shigella* vaccines and the computer-aided engineering of carbohydrate-active enzymes.[44] In particular, the now established RT and AT specific parameters of each glucosylated ABC′D′ of interest combined to the high resolving power and reproducibility of UHPLC−IMS/IMS provide a reproducible and sensitive medium throughput stand-alone method for the screening of improved SF-specific biocatalysts. Obviously, the strategy exemplified herein could be extended to numerous screening applications.

Most notably, our results also demonstrate the potential and complementarity of IMS/IMS and CTD, two recently introduced major technological advances in the demanding field of structural/analytical glycosciences. By merging the capacities to separate and manipulate ions in high-resolution IMS/IMS and the comprehensiveness of the structural information available by CTD, we were able to investigate the structural diversity of molecules present in very low amounts in complex mixtures. Beyond the structural identification of multiple glycoforms co-existing in biological samples, we also demonstrate that this highly sensitive technology allows the structural elucidation of minor contaminants present in synthesized compounds to an extent that may not be achieved otherwise. We propose that the combination of IMS/IMS and CTD could turn into an attractive accurate method for the control quality of glycan-based active ingredients. In order to further improve the capabilities of the two methods, a setup combining high-resolution ion mobility and high-energy fragmentation would be a platform of choice for these approaches.

ASSOCIATED CONTENT

Supporting Information

The Supporting Information is available free of charge at https://pubs.acs.org/doi/10.1021/acs.analchem.1c04982.

Scheme of the strategy used for IMS/IMS analysis; extracted ion chromatogram of the LC−MS analysis of sample M30; UHPLC−MS spectra of the six pentasaccharide isomers of interest separated in sample M30; extracted ion mobility spectrum at *m/z* 1062.2 for all reaction samples after UHPLC−IMS separation; 2D map of the UHPLC separation of sample M41 with different number of/multiple passes; annotation of the 2D map obtained by UHPLC−IMS/IMS−MS for each reaction sample; correlation between the 2D map of the UHPLC−IMS/IMS−MS separation and the UHPLC−MS analysis of sample M18; and UHPLC-He-CTD spectra of each of the eight pentasaccharide isomers (PDF)

AUTHOR INFORMATION

Corresponding Author

Hélène Rogniaux − *INRAE, UR BIA, F-44316 Nantes, France; INRAE, BIBS Facility, F-44316 Nantes, France;*

orcid.org/0000-0001-6083-2034;
Email: helene.rogniaux@inrae.fr

Authors

David Ropartz − *INRAE, UR BIA, F-44316 Nantes, France; INRAE, BIBS Facility, F-44316 Nantes, France;* orcid.org/0000-0003-4767-6940

Mathieu Fanuel − *INRAE, UR BIA, F-44316 Nantes, France; INRAE, BIBS Facility, F-44316 Nantes, France;* orcid.org/0000-0001-8384-8266

Simon Ollivier − *INRAE, UR BIA, F-44316 Nantes, France; INRAE, BIBS Facility, F-44316 Nantes, France;* orcid.org/0000-0002-7671-1736

Adrien Lissarrague − *INRAE, UR BIA, F-44316 Nantes, France; INRAE, BIBS Facility, F-44316 Nantes, France*

Mounir Benkoulouche − *Toulouse Biotechnology Institute, TBI, Université de Toulouse, CNRS, INRAE, INSA, F-31077 Toulouse Cedex 04, France*

Laurence A. Mulard − *Institut Pasteur, Université de Paris, CNRS UMR3523, Unité de Chimie des Biomolécules, 75724 Paris Cedex 15, France;* orcid.org/0000-0002-5622-1422

Isabelle André − *Toulouse Biotechnology Institute, TBI, Université de Toulouse, CNRS, INRAE, INSA, F-31077 Toulouse Cedex 04, France;* orcid.org/0000-0001-6280-4109

David Guieysse − *Toulouse Biotechnology Institute, TBI, Université de Toulouse, CNRS, INRAE, INSA, F-31077 Toulouse Cedex 04, France*

Complete contact information is available at: https://pubs.acs.org/10.1021/acs.analchem.1c04982

Author Contributions

D.R., M.F., and H.R. conceived the study. D.R. performed the experiments. A.L. optimized the experimental parameters for He-CTD. S.O. optimized the experimental parameters for IMS. M.B., L.A.M., I.A., and D.G. provided the materials/samples to be analyzed D.R., M.F., and H.R. interpreted the results. The manuscript was written through contributions of all authors. All authors have approved the final version of the manuscript.

Notes

The authors declare no competing financial interest.

■ ACKNOWLEDGMENTS

This work was partially funded by the French National Research Agency (grant ANR-15-CE07-0019 and grant ANR-18-CE29-0006).

■ REFERENCES

(1) Laine, R. A. *Glycobiology* **1994**, *4*, 759−767.
(2) Gabius, H.-J.; Cudic, M.; Diercks, T.; Kaltner, H.; Kopitz, J.; Mayo, K. H.; Murphy, P. V.; Oscarson, S.; Roy, R.; Schedlbauer, A.; Toegel, S.; Romero, A. What Is the Sugar Code? *ChemBioChem* 2021.
(3) Varki, A. *Glycobiology* **2017**, *27*, 3−49.
(4) Reily, C.; Stewart, T. J.; Renfrow, M. B.; Novak, J. *Nat. Rev. Nephrol.* **2019**, *15*, 346−366.
(5) Poole, J.; Day, C. J.; von Itzstein, M.; Paton, J. C.; Jennings, M. P. *Nat. Rev. Microbiol.* **2018**, *16*, 440−452.
(6) Dhar, P.; McAuley, J. *Infect. Microbiol.* **2019**, *9*, 117.
(7) Sharma, S.; Shekhar, S.; Sharma, B.; Jain, P. *RSC Adv.* **2020**, *10*, 34099−34113.
(8) Rappuoli, R. *Sci. Transl. Med.* **2018**, *10*, No. eaat4615.
(9) Barel, L.-A.; Mulard, L. A. *Hum. Vaccines Immunother.* **2019**, *15*, 1338−1356.
(10) Anderluh, M.; Berti, F.; Bzducha-Wrobel, A.; Chiodo, F.; Colombo, C.; Compostella, F.; Durlik, K.; Ferhati, X.; Holmdahl, R.; Jovanovic, D.; Kaca, W.; Lay, L.; Marinovic-Cincovic, M.; Marradi, M.; Ozil, M.; Polito, L.; Reina, J. J.; Reis, C. A.; Sackstein, R.; Silipo, A.; Svajger, U.; Vanek, O.; Yamamoto, F.; Richichi, B.; van Vliet, S. J. *FEBS J.* **2021**, DOI: 10.1111/febs.15909. , Early Access
(11) van der Put, R. M. F.; Kim, T. H.; Guerreiro, C.; Thouron, F.; Hoogerhout, P.; Sansonetti, P. J.; Westdijk, J.; Stork, M.; Phalipon, A.; Mulard, L. A. *Bioconjugate Chem.* **2016**, *27*, 883−892.
(12) Cohen, D.; Atsmon, J.; Artaud, C.; Meron-Sudai, S.; Gougeon, M.-L.; Bialik, A.; Goren, S.; Asato, V.; Ariel-Cohen, O.; Reizis, A.; Dorman, A.; Hoitink, C. W. G.; Westdijk, J.; Ashkenazi, S.; Sansonetti, P.; Mulard, L. A.; Phalipon, A. *Lancet Infect. Dis.* **2021**, *21*, 546−558.
(13) Reyes, C. D. G.; Jiang, P.; Donohoo, K.; Atashi, M.; Mechref, Y. S. *J. Sep. Sci.* **2021**, *44*, 403−425.
(14) Giles, K.; Pringle, S. D.; Worthington, K. R.; Little, D.; Wildgoose, J. L.; Bateman, R. H. *Rapid Commun. Mass Spectrom.* **2004**, *18*, 2401−2414.
(15) Tolmachev, A. V.; Webb, I. K.; Ibrahim, Y. M.; Garimella, S. V. B.; Zhang, X.; Anderson, G. A.; Smith, R. D. *Anal. Chem.* **2014**, *86*, 9162−9168.
(16) Wojcik, R.; Nagy, G.; Attah, I. K.; Webb, I. K.; Garimella, S. V. B.; Weitz, K. K.; Hollerbach, A.; Monroe, M. E.; Ligare, M. R.; Nielson, F. F.; Norheim, R. V.; Renslow, R. S.; Metz, T. O.; Ibrahim, Y. M.; Smith, R. D. *Anal. Chem.* **2019**, *91*, 11952−11962.
(17) Deng, L.; Webb, I. K.; Garimella, S. V. B.; Hamid, A. M.; Zheng, X.; Norheim, R. V.; Prost, S. A.; Anderson, G. A.; Sandoval, J. A.; Baker, E. S.; Ibrahim, Y. M.; Smith, R. D. *Anal. Chem.* **2017**, *89*, 4628−4634.
(18) Nagy, G.; Attah, I. K.; Garimella, S. V. B.; Tang, K.; Ibrahim, Y. M.; Baker, E. S.; Smith, R. D. *Chem. Commun.* **2018**, *54*, 11701−11704.
(19) Giles, K.; Wildgoose, J.; Pringle, S.; Garside, J.; Carney, P.; Nixon, P.; Langridge, D. Design and Utility of a Multi-Pass Cyclic Ion Mobility Separator. *In Annual Conference Proceedings*; ASMS: Baltimore, 2014.
(20) Giles, K.; Ujma, J.; Wildgoose, J.; Pringle, S.; Richardson, K.; Langridge, D.; Green, M. *Anal. Chem.* **2019**, *91*, 8564−8573.
(21) Eldrid, C.; Thalassinos, K. *Biochem. Soc. Trans.* **2020**, *48*, 2457−2466.
(22) Ujma, J.; Ropartz, D.; Giles, K.; Richardson, K.; Langridge, D.; Wildgoose, J.; Green, M.; Pringle, S. *J. Am. Soc. Mass Spectrom.* **2019**, *30*, 1229−1240.
(23) Ropartz, D.; Fanuel, M.; Ujma, J.; Palmer, M.; Giles, K.; Rogniaux, H. *Anal. Chem.* **2019**, *91*, 12030−12037.
(24) Ollivier, S.; Tarquis, L.; Fanuel, M.; Li, A.; Durand, J.; Laville, E.; Potocki-Veronese, G.; Ropartz, D.; Rogniaux, H. *Anal. Chem.* **2021**, *93*, 6254−6261.
(25) Ollivier, S.; Fanuel, M.; Rogniaux, H.; Ropartz, D. *Anal. Chem.* **2021**, *93*, 10871−10878.
(26) Sanda, M.; Morrison, L.; Goldman, R. *Anal. Chem.* **2021**, *93*, 2003−2009.
(27) Dyukova, I.; Faleh, A. B.; Warnke, S.; Yalovenko, N.; Yatsyna, V.; Bansal, P.; Rizzo, T. R. *Analyst* **2021**, *146*, 4789−4795.
(28) Chen, X.; Wang, Z.; Wong, Y.-L. E.; Wu, R.; Zhang, F.; Chan, T.-W. D. *Mass Spectrom. Rev.* **2018**, *37*, 793−810.
(29) Brodbelt, J. S.; Morrison, L. J.; Santos, I. *Chem. Rev.* **2020**, *120*, 3328−3380.
(30) Ropartz, D.; Li, P.; Fanuel, M.; Giuliani, A.; Rogniaux, H.; Jackson, G. P. *J. Am. Soc. Mass Spectrom.* **2016**, *27*, 1614−1619.
(31) Ropartz, D.; Li, P.; Jackson, G. P.; Rogniaux, H. *Anal. Chem.* **2017**, *89*, 3824−3828.
(32) Buck-Wiese, H.; Fanuel, M.; Liebeke, M.; Le Mai Hoang, K.; Pardo-Vargas, A.; Seeberger, P. H.; Hehemann, J.-H.; Rogniaux, H.; Jackson, G. P.; Ropartz, D. *J. Am. Soc. Mass Spectrom.* **2020**, *31*, 1249−1259.
(33) Pepi, L. E.; Sasiene, Z. J.; Mendis, P. M.; Jackson, G. P.; Amster, I. J. *J. Am. Soc. Mass Spectrom.* **2020**, *31*, 2143−2153.

(34) Benkoulouche, M.; Ben Imeddourene, A.; Barel, L.-A.; Lefebvre, D.; Fanuel, M.; Rogniaux, H.; Ropartz, D.; Barbe, S.; Guieysse, D.; Mulard, L. A.; Remaud-Siméon, M.; Moulis, C.; André, I. *Sci. Rep.* **2021**, *11*, 20294.
(35) Benkoulouche, M.; Imeddourene, A. B.; Barel, L.-A.; Le Heiget, G.; Pizzut, S.; Kulyk, H.; Bellvert, F.; Bozonnet, S.; Mulard, L. A.; Remaud-Siméon, M.; Moulis, C.; André, I. *Sci. Rep.* **2021**, *11*, 2474.
(36) Khalil, I. A.; Troeger, T.; Blacker, B. F. *Lancet Infect. Dis.* **2018**, *18*, 1305.
(37) Walker, R.; Kaminski, R. W.; Porter, C.; Choy, R. K. M.; White, J. A.; Fleckenstein, J. M.; Cassels, F.; Bourgeois, L. *Microorganisms* **2021**, *9*, 1382.
(38) Hu, Z.; Benkoulouche, M.; Barel, L.-A.; Le Heiget, G.; Imeddourene, A. B.; Le Guen, Y.; Monties, N.; Guerreiro, C.; Remaud-Siméon, M.; Moulis, C.; André, I.; Mulard, L. A. *J. Org. Chem.* **2021**, *86*, 2058−2075.
(39) Hoffmann, W. D.; Jackson, G. P. *J. Am. Soc. Mass Spectrom.* **2014**, *25*, 1939−1943.
(40) Kessner, D.; Chambers, M.; Burke, R.; Agus, D.; Mallick, P. *Bioinformatics* **2008**, *24*, 2534−2536.
(41) Niedermeyer, T. H. J.; Strohalm, M. *PLoS One* **2012**, *7*, No. e44913.
(42) Perepelov, A. V.; Shekht, M. E.; Liu, B.; Shevelev, S. D.; Ledov, V. A.; Senchenkova, S. y. N.; L'vov, V. L.; Shashkov, A. S.; Feng, L.; Aparin, P. G.; Wang, L.; Knirel, Y. A. *FEMS Immunol. Med. Microbiol.* **2012**, *66*, 201−210.
(43) Knirel, Y. A.; Sun, Q.; Senchenkova, S. N.; Perepelov, A. V.; Shashkov, A. S.; Xu, J. *Biochemistry* **2015**, *80*, 901−914.
(44) Wang, Y.; Xue, P.; Cao, M.; Yu, T.; Lane, S. T.; Zhao, H. *Chem. Rev.* **2021**, *121*, 12384−12444.